FRAGILITY CURVE PROBABILISTIC MODEL APPLIED TO DURABILITY AND LONG TERM MECHANICAL DAMAGE OF MASONRY

Elsa Garavaglia[1], Anna Anzani[1], Luigia Binda[2], Giuliana Cardani[3]

1. INTRODUCTION

During their service life, masonry structures can be subjected to decay due to environmental attacks, aging and/or damage due to long term heavy loads.

Salts crystallising behind the surface cause delamination and crumbling of the masonry components and are one of the most frequent causes of damage to masonry walls in many environments.

Together with other synergetic aspects, including the intrinsic weakness of poorly connected multiple masonry leaves, time dependent behaviour has proved to be involved in collapses occurred during the last twenty years.

The great randomness associated in each decay phenomena suggests to study these processes from a probabilistic point of view. The deterioration of masonry materials and the long term behaviour of ancient buildings have therefore been investigated through a simple probabilistic approach aimed to the prediction of the time needed to reach a given level of damage, that is an important issue in planning strategies for the maintenance and repair of existing buildings.

The model has been applied to interpret sets of experimental data collected on: (i) samples of masonry (wallettes) subjected to salt crystallisation and tested in laboratory through accelerated aging tests and (ii) samples of historic masonry subjected to laboratory creep and pseudo creep tests.

The probabilistic approach in its theoretical form is presented in section 2. The applications to material deterioration and to the long term behaviour of ancient masonry are presented in section 3 and section 4 respectively. In section 4.4 the first application of this procedure to a real case is proposed.

2. FRAGILITY CURVE FOR SERVICE LIFE PREDICTION

In view of the preservation of the Cultural Heritage toward different causes of physical and mechanical damage, the probability that a system will reach, or exceed, a given damage threshold over time often requires to be evaluated. According to the specific damage process that in turn is analyzed, this threshold may correspond to the thickness of the lost surface material due to salt decay (Section 3), the strain-rate induced by the creep behaviour (Section 4) or other significant parameters.

Therefore, a parameter ℓ defined as the loss of performance reached by the system at the time t^* has to be chosen to describe the deterioration process of porous materials. The high randomness associated with the occurrence of the decay of a structural system in the natural environment justifies the consideration of ℓ as a random variable (r.v.) with a certain probability distribution (Binda et al. 1999*b*). Since the deterioration depends on the instant t^* in which it is recorded, at each time t^* the loss ℓ can be modelled with a probability density function (p.d.f.) $f_\ell(L)$ which depends not only on the r.v. ℓ, but also on the constant parameter t^* (Fig. 1*a*). From this point of view, the deterioration process can be considered as a stochastic process of the r.v. ℓ. In order to

[1] *Associate Professor, Department of Structural Engineering, Politecnico of Milan, Piazza L. da Vinci, 32, 20133 MILANO, Italy.*

[2] *Full Professor, Department of Structural Engineering, Politecnico of Milan, Piazza L. da Vinci, 32, 20133 MILANO, Italy.*

[3] *Assistant Professor, Department of Structural Engineering, Politecnico of Milan, Piazza L. da Vinci, 32, 20133 MILANO, Italy.*

model $f_\ell(L)$, a theoretical distribution needs to be chosen at every time *t**. Obviously, the distribution modelling a given phenomenon must be chosen on the basis of the physical aspects of the phenomenon itself, and of the characteristics of the distribution function in its "tail", where experimental results are scarce. The most suitable distribution function can be chosen analyzing at every time *t** the behaviour of the failure rate function $\phi_\ell(L)$ connected to the distribution function itself (details are given in Garavaglia et al. 2004*b*):

$$\phi_\ell(L)dL = \Pr\left\{L < \ell \le L + dL \,\middle|\, \ell > L\right\} = \frac{f_\ell(L)}{1 - F_\ell(L)} \qquad \forall\ t^* \tag{1}$$

where, as said above, Pr denotes the *conditioned probability of failure*, $f_\ell(L)$ is the probability density function and $F_\ell(L)$ the cumulative distribution of the r.v. ℓ.

The behaviour of $\phi_\ell(L)$ defines the *immediate* failure rate *dL;* if the event has not yet happened at $\ell = L$, then three possibilities are given:

- a constant $\phi_\ell(L)$ means that the probability of an immediate occurrence of the next failure *dL* is always the same and is not affected by the reached level of loss *L*; this is the typical Poisson process and can describe the loss of performance due to the aging when no other factors play a particular role in it. A distribution characterized by this $\phi_\ell(L)$ is the Exponential;
- a decreasing $\phi_\ell(L)$ means that the probability of an immediate occurrence of the next failure *dL* decreases when the reached level of loss *L* increases; this seems to happen in the delamination phenomenon where the thickness of the detached layers is always lower than a characteristic values. A distribution characterized by this $\phi_\ell(L)$ is the Lognormal distribution;
- an increasing $\phi_\ell(L)$ means that if the material has already reached a given loss of performance *L* and the loss $\ell > L$ has not yet happened, the probability to have a failure in the next *dL* increases if the reached level of loss *L* increases. At *L* tending to infinite, $\phi_\ell(L)$ can increase either tending to infinite or tending to an asymptotic value; both situations are typical of the extreme value distributions. By experimental evidence the strain rate vs. stress phenomenon (Sect. 4) seems to obey to this model, in particular it seems to tend to infinite when the stress increases over a certain level.

According to Eq. 1 and to the studied physical problems, different distributions have been chosen: in particular a Lognormal distribution in the case of salt crystallization process and a Weibull distribution in the case of creep induced damage.

Considering a significant damage $\overline{\ell}$ and the variable time needed to exceed it, a physical or mechanical deterioration process can be treated as a reliability problem (Garavaglia et al. 2002).

Reliability *R*(*t*) is related to the performance of a system over time, and is defined as the probability that the system does not fail by time *t* (Evans 1992). This definition is extended here, denoting by $\overline{R}(t)$ the probability that a system will exceed a given significant damage threshold $\overline{\ell}$ by time *t.* The random variable used to quantify reliability is $\overline{T}$, which is simply the time taken to exceed the damage $\overline{\ell}$. Thus, from this point of view, the reliability function is given by:

$$\overline{R}(t) = \Pr(\overline{T} > t) = 1 - F_{\overline{T}}(t) \tag{2}$$

where $F_{\overline{T}}(t)$ is the distribution function for $\overline{T}$. Assuming that the density function $f_{\overline{T}}(t)$ exists for the r.v. $\overline{T}$, the failure rate function $\phi_{\overline{T}}(t)$ is given by (Evans 1992):

$$\phi_{\overline{T}}(t) = \frac{f_{\overline{T}}(t)}{\overline{R}(t)} \tag{3}$$

Computing $F_{\overline{T}}(t)$ for different damage levels $\overline{\ell}$ allows us to build the *fragility curve* for each $\overline{\ell}$.

A fragility curve describes the probability of reaching or exceeding a given damage $\bar{\ell}$ over time (Singhal at al. 1996). At a given time *t**, the probability that a particular damage level $\bar{\ell}$ will be reached can be seen as the area below the threshold $\bar{\ell}$ and the probability that it is exceeded can be seen as the area above the threshold $\bar{\ell}$ (Fig. 1*a*) (Garavaglia et al., 2002*b,* Garavaglia et al., 2004*b*). The latter area can be calculated by using the survive function:

$$\Im_{\ell}(L) = 1 - F_{\ell}(L) \qquad \forall \quad t^* \tag{4}$$

where $F_{\ell}(L)$ is the cumulative distribution function of the probability density function p.d.f. chosen to model the parameter ℓ at every *t**. The computation of $\Im_{\ell}(L)$ at every *t** is performed by means of numerical integration. For each chosen damage threshold $\bar{\ell}$, the areas computed provide the *experimental fragility curves* $F_{\bar{T}^*}(t)$ at different *t** (Fig. 1*b*).

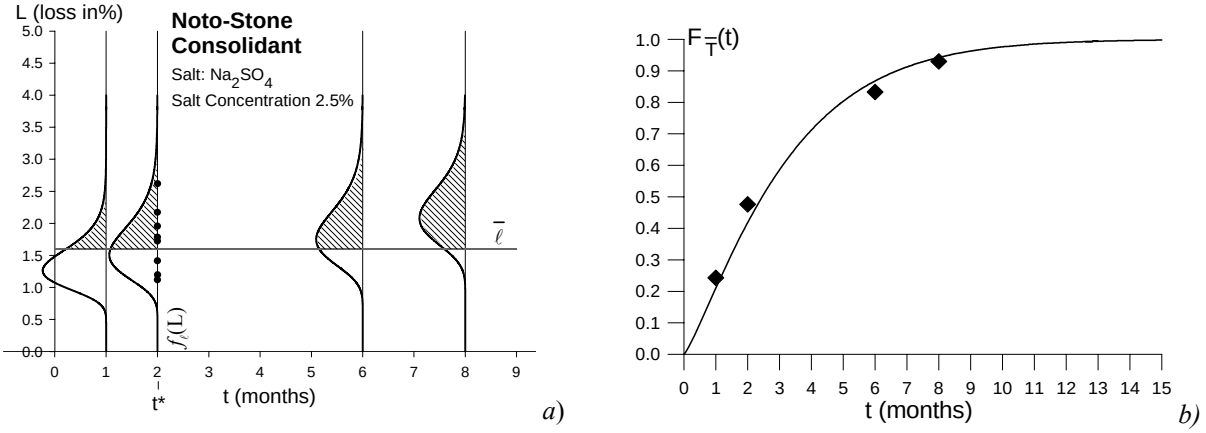

Figure 1. Probability to cross the threshold $\bar{\ell}$ *: a) Lognormal p.d.f. modelling damage at each t*; b) experimental* (♦) *and Weibull theoretical* (—) *fragility curves.*

Also to model numerically the experimental fragility curves, a function has to be chosen that should provide a good interpretation of the physical phenomenon: in all the damage cases studied here, a Weibull distribution has been chosen (Cranmer et al. 1998, Bekker 1999, Garavaglia et al., 2002*b*, Garavaglia et al. 2004*b*):

$$F_{\bar{T}}(t) = 1 - \exp\left[-(\rho\, t)^{\alpha}\right] \tag{5}$$

In fact, the failure rate function $\phi_{\bar{T}}(t)$ has a polynomial form and, consequently, must be (Garavaglia et al. 2002*b*, Garavaglia et al., 2004*b*):

$$\phi_{\bar{T}}(t) = b_1 t^{b_2} \tag{6}$$

where $b_1 > 0$ and $-1 < b_2 < +\infty$ are constant.
Since using eq. (2):

$$\overline{R}(t) = \exp\left\{-\int_0^t \phi_{\bar{T}}(u)du\right\} \tag{7}$$

and

$$f_{\bar{T}}(t) = \phi_{\bar{T}}(t)\exp\left\{-\int_0^t \phi_{\bar{T}}(u)du\right\} \tag{8}$$

and assuming: $b_1 = \alpha\rho^{\alpha}$ and $b_2 + 1 = \alpha$ (with constant α and ρ), then:

$$\int_0^t \phi_{\bar{T}}(u)du = \frac{b_1 t^{b_2+1}}{b_2+1} = (\rho\, t)^{\alpha} \tag{9}$$

Therefore, by Eq. 6 and Eq. 7:

$$\overline{R}(t) = \exp[-(\rho\, t)^{\alpha}] \tag{10}$$

and

$$f_{\overline{T}}(t) = \alpha\rho(\rho\, t)^{\alpha-1} \exp[-(\rho\, t)^{\alpha}] \tag{11}$$

which is definitely the well known p.d.f. of Weibull distribution (Cox, 1962, Evans, 1992).

3. THE LIFETIME PREDICTION FOR MASONRY DETERIORATED THROUGH LABORATORY AGING TESTS

Structures subjected to aggressive environments may suffer degradation of their component materials during their service life. The presence of moisture in the walls, due to capillary rise and/or rain penetration, is the vehicle through which soluble salts are distributed in the material.

It should be considered that when the delamination/crumbling reaches a certain threshold $\overline{\ell}$, the characteristics of a porous material and hence the reliability of the system could be seriously impaired. But, when will this threshold be reached? And how can the damage be quantified?

The problem of quantifying surface damage without destructive testing and of monitoring its evolution in time without excessively long tests is an open question. The objective of this research has been to develop a procedure that can predict, in probabilistic terms, the evolution of surface decay in time, without a large set of experimental data.

The durability of bricks toward salt crystallisation decay is largely influenced by the mortar, according to the porosity characteristics of the two materials. Therefore, when the prediction of masonry durability is required, long term and hence costly durability tests on single masonry components, brick, stone or mortar are of very limited utility (Binda & Baronio, 1985; Binda et al., 1985, Van Hees et al., 1996). According to a crystallisation test on wallettes made of units assembled with mortar, set up by TNO (Delft, NL) and included in the RILEM MS A.1, 1998 Recommendation, experimental data have been recorded in both indoor (Binda et al., 1985) and outdoor laboratories (Berra et al., 1993) over a number of years forming a fundamental data-set on the investigation on reliability of masonry materials in time.

Considering that the great complexity of the environmental processes causing material deterioration can not be completely reproduced in the laboratory, the adoption of appropriate probabilistic modelling for a better interpretation of the phenomena seems to be a good approach (Binda et al., 1990*b*, Cranmer et al., 1998, Bekker, 1999).

3.1. Laboratory Aging Tests

Durability tests are aimed to: reproducing the site situation, evaluating the resistance of the materials to deterioration, preventing damage, design and quality control. Applying surface treatments to prevent masonry decay is an easy and common, but costly, practice which is thought to avoid or reduce masonry damage and hence delay the ordinary maintenance. Research carried out in the past (Binda et al. 1992) concluded that water proof and consolidant surface treatments of porous material in the presence of soluble salts induce the detachment of the whole treated parts due to the possible formation of cryptoefflorescences.

Within an EC Contract (ENV4-CT98-0710), an attempt has been made to individuate the maximum allowable salt content in brick and stone masonry, below which the surface protection treatments do not fail. Crystallisation tests following RILEM TC 127 MS Recommendation were carried out at the Dept. of Struct. Engineering Politecnico of Milan on treated and untreated brick and limestone masonry specimens (Cardani et al., 2002) (Fig. 2). A large number of tests had previously been carried out on the single units used for the masonry specimens (Garavaglia et al., 2002*a*). Salt solutions with two low concentrations of sodium sulphate (1% and 2,5% of the

measured capillary moisture content, referred to the % weight of the dry specimen) were introduced in masonry wallettes treated with a water based water repellent (solventless silicone microemulsion concentrate based on silanes and siloxanes) or with a consolidant (reactive silicic acid ethyl ester compounds). A saturated salt solution as indicated by the RILEM recommendation was not used, because the aim was to define a salt content threshold for treatments. The aging test was carried out in an environment of 20°C and 50% R.H. on masonry wallettes (250x200x120 mm) made with softmud bricks and on masonry wallettes built with natural stones: Noto limestone, Savonnière stone and Serena sandstone. The wallettes were all prepared with bedding joints, 15 mm thick, made with a putty lime based mortar (Cardani et al. 2002).

3.1.1. Monitoring and Quantification of the Damage

The test chosen is useful to study the performance of the brick(stone)/mortar systems in the laboratory, with and without surface treatments. In order to gain significant results from crystallisation tests, the monitoring time needs to be sufficiently long (6 months or more) and the number of cycles, corresponding to a new water supply after complete evaporation of the system, must be not less than three.

Salt crystallization produces high stresses inside the material and results in a continuous crumbling and delamination of the external surface of the wall, the material underneath remaining unaltered. The loss of material as a function of time is a good measure that can be adopted as a damage parameter in the case of salt decay of porous surfaces (Binda et al, 1992). Therefore, the variation of subsequent surface profile has been assumed as a measure of damage and a laser profilometer used for its monitoring in time (Fig. 3) (Berra et al., 1993, Baronio et al, 1993 and Cardani et al., 2002).

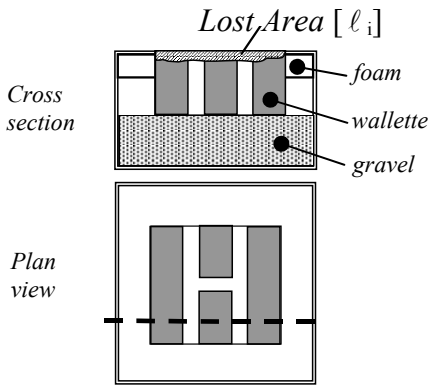

Figure 2. Box scheme for the crystallisation tests, following RILEM TC 127 MS Recommendation.

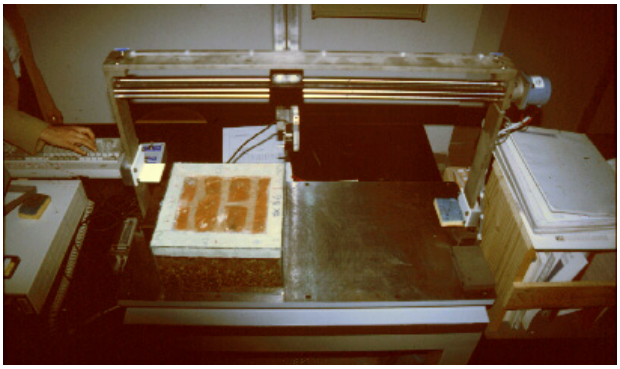

Figure 3. Laser profilometer device during measurement.

The device allows to draw plots of the surface profile in chosen positions. Subsequent measurements show how the profile changes due to any superficial decay and allow to measure the material loss in time. Figure 4 shows four example surface profiles for four different measurements. Since bulging (or swelling) occurs at a step before delamination, this can be considered as the onset of damage. The experimental measurements need to be converted into new deterioration diagrams where bulging has been eliminated; this has permitted to quantify correctly the swelled material as a "loss". The procedure compares the vertical co-ordinates of two subsequent diagrams: the current plot n and the previous plot ($n-1$). The co-ordinates of the diagram n are usually lower than those of the diagram ($n-1$), except for the points affected by swelling. In these points the computer code continues the procedure, comparing the co-ordinates of plot n with those of the subsequent plots ($n+1$), ($n+2$), ($n+3$) …until a plot $m=(n+i)$ having lower vertical values than that of profile n is found. The co-ordinates of diagram m, corresponding to the points affected by bulging, become the new reference co-ordinates of profile n when redrawn. As a result, a clean plot of the evolution of the surface damage as a function of time and space is obtained (Fig. 4*b*) (Garavaglia et al. 2002*a*).

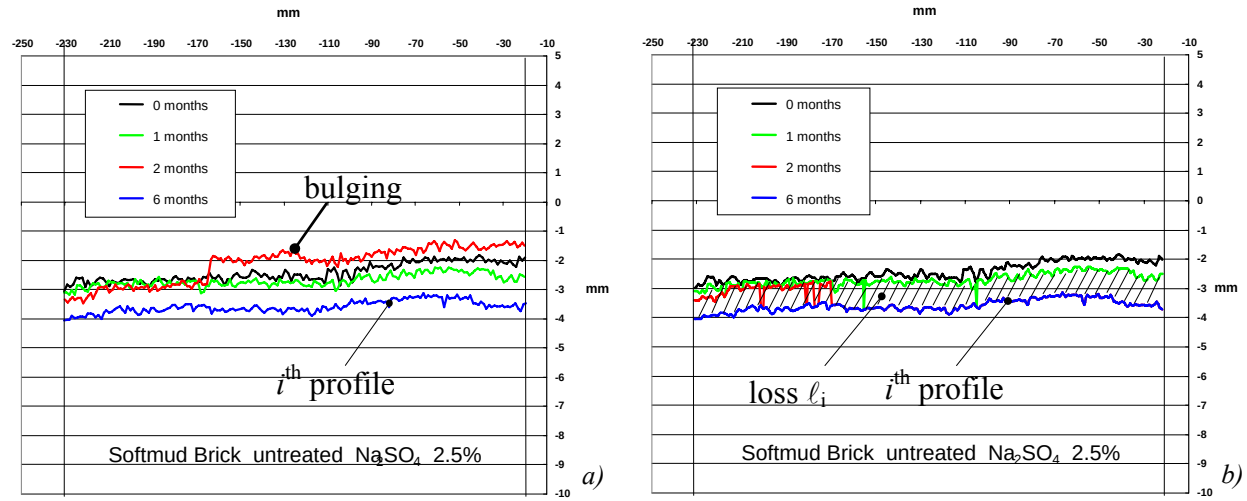

Figure 4a, b. Example of deterioration measurements over time
a) before and b) after the swelling has been removed on a unit of the masonry specimen.

The loss of material can be quantified using the new diagrams of Fig. 4*b*. Therefore, for each profile *i* represented in Fig. 4*b*, the loss ℓ_i of cross section of the wallette (in mm^2), calculated at every measurement time t^* (t^*= 0, 1, 2, 6 months), has been assumed as the damage parameter. To quantify ℓ_i, the area included between two consecutive diagrams is calculated at every time t^* (Fig. 4*b*). This area is automatically calculated by the computer code studied to eliminate bulging by means of the composite trapezoidal rule (Garavaglia et al. 2002*a*).

3.2 Stochastic Modelling of the Deterioration Process

The parameter ℓ, describing the surface deterioration process of porous materials, can be defined as the loss of performance reached by the system at the time t^*.

To compare all the experimental results obtained during the period required by the EC Contract, the damage has been plotted in percentage:

$$L = \frac{\text{lost area}}{\text{area of section}} \cdot 100 \qquad (12)$$

In Fig. 5, where the readings at 8 months have been reported in addition to the data of Figure 4, a simple interpolation of the experimental points permits to better read the loss trend ℓ_i over time (linear splices).

As mentioned before, at each time t^* the loss ℓ can be modelled with a probability density function (p.d.f.) $f_\ell(L)$ depending on ℓ and the constant parameter t^* = 0, 1, 2, 6, 8, months. In order to model $f_\ell(L)$, a theoretical distribution needs to be chosen at every time t^*. Usually, the recorded experimental data collected by monitoring deteriorating structures show dispersion around the average value of ℓ. However, the loss of performance seems to be contained within a certain range of values. Therefore, it seems correct to assume that, at a given time t^*, the probability of a loss $(L < \ell \le L + dL)$ decreases as the value L (magnitude of the loss) increases. This assumption can be made as a good – although not unique – physical interpretation of the decay process. Analysing the failure rate function Eq. 1, a Lognormal p.d.f. looks like the most suitable choice to model ℓ in this case (Fig. 5), as follows:

$$f_\ell(L) = \frac{1}{L\sqrt{(2\pi\omega)}} \exp\left\{-\frac{[\log(\eta L)]^2}{2\omega}\right\} \quad \forall\ t^* \qquad (13)$$

where ω and η are the parameters of the distribution.

The parameters of the distribution in Eq. 13 have been estimated through a computer code using the maximum likelihood method and the Rosenbrock's optimization method (IMSL Fortran

Library). As suggested in (Maybech, 1979) to estimate the parameters of a density distribution (Eqs. 13 and 14) this method is preferable than the least squares method (more details in Maybech, 1979 and Augusti et al. 1984). On the contrary, to estimate the parameters of a cumulate distribution (Eq. 5) the least squares method and the Rosenbrock's optimization method have been preferred. This estimation approach has been used, with good results, to evaluate the parameters of all the distribution used here below.

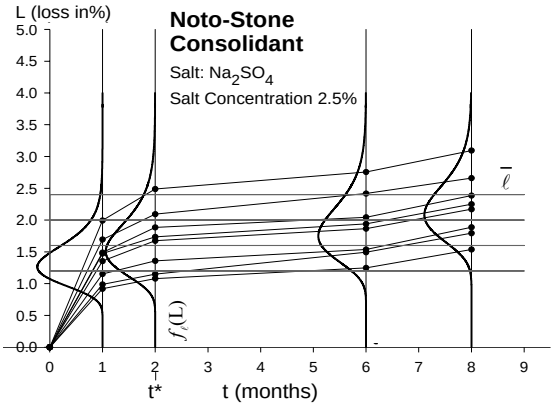

Figure 5. Probability to cross the threshold $\bar{\ell}$: interpolation of the loss diagrams (*) and LogN p.d.f

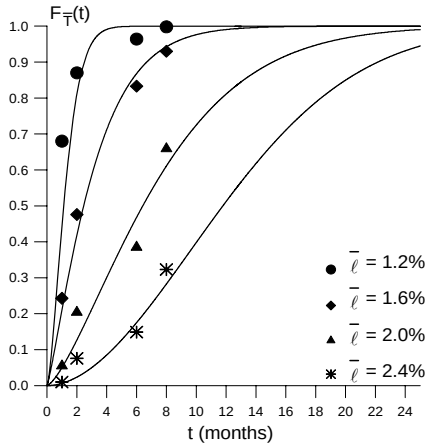

*Figure 6. Experimental (●, ▲, ♦, *) and theoretical (Weibull) fragility curves (—)*

Through the fragility curves obtained by computing Equation 4 (experimental fragility curves) and Equation 5 (theoretical fragility curves), it is possible to identify the failures with a higher or lower probability of occurrence in the given time *t* (Fig. 6).

3.3 The Probabilistic Approach Applied to crystallization tests

The fragility curves on the results of the crystallisation test with the highest Na_2SO_4 concentration carried out on softmud brick wallettes are reported in Figure 7, where a comparison between the effect of the two treatments and the untreated reference is made.

By visual inspection, the damage of the untreated reference wallette with the lowest concentration (1%) was very poor in the first three months and then started uniformly. With the highest concentration of 2.5 % of Na_2SO_4, the damage raised rapidly in the first two/three weeks, due to efflorescence and cryptoflorescence, in both materials: bricks and mortar. The consolidant treatment led to cryptoefflorescence under the treated layer; the damage started in the brick and then diffused to the mortar. The treated bricks presented some spalling of the surface: a first layer with a thickness of 2-3 mm after 6 weeks and a second layer with a thickness of 1.2 mm after 8 months (Fig. 7*b*). On the contrary, the water repellent did not produce on the bricks any visible damage within a period of 8 months, which was largely visible only on the mortar joints.

Through the fragility curves approach, the magnitude of the expected damage over time and its occurrence time was predicted. The optimised estimation of the distributions parameters was obtained by fitting the experimental fragility curves; the error in the parameter estimation has been calculated by least squares method through optimisation: of course it varies with the test modelled. For the fragility curves modelled in Figure 7*a* the values of the error are included within a very small range (1.1e-12 – 2.0e-08); referring to Figure 7*b* values of the the error are included within the interval 7.0e-05 – 6.97e-03; for the modelling of Figure 7*c* the maximum error value is 3.52e-04.

For the untreated wallettes and the wallettes treated with consolidant, the fragility curves permit the comparison between the exceedance probability to pass different thresholds $\bar{\ell} = 1.2\%$ and $\bar{\ell} = 1.6\%$ of material loss. In Figure 7*a* the untreated system presents a very high probability (close to 100%) to reach or exceed the damage level $\bar{\ell} = 1.2\%$ in a short time (less than 2 months). On the

contrary, the system treated with consolidant shows the same high probability to reach the threshold $\bar{\ell} = 1.2\%$ in around 12 months (Fig. 7*b*). Related to the threshold $\bar{\ell} = 1.6\%$, in Figure 7*a* the system shows a high probability to reach this damage level in around 8-10 months; vice-versa, for the system in Figure 7*b* the same probability is reached after 24 months. The presence of consolidant seems to protect the brick masonry surface, but given the continuous supply of rising damp with salt solution the protective action vanishes after a short period of time.

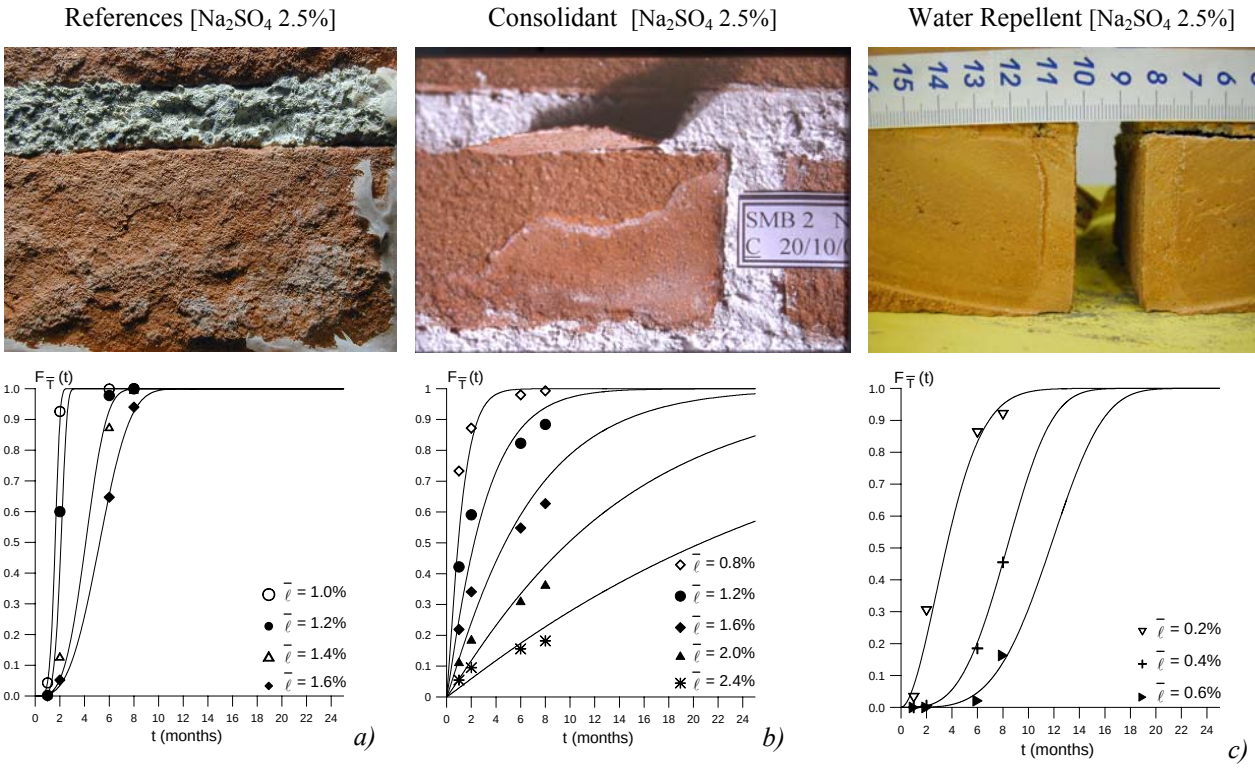

Figure 7. Fragility curves built on Softmud brick masonry specimens with different surface treatments.

The wallette surfaces treated with the water repellent benefited of the protective action during the entire testing time. Thus, the fragility curves for the wallette with water repellent are referred only to a low level of damage (not greater than 0.6% of loss). For estimating higher levels, the test should have continued longer, but this would have overcome the Contract duration. After cutting the specimen treated with water repellent at 2.5% of salt concentration, a small white line of salt appeared clearly underneath the treated layer (Fig. 7*c*). Since the mortar is the only vehicle to water evaporation, the mortar joints are the first material to be damaged. According to previous experiences and to the assumed model, the decay of these bricks can be expected within two or three years. Of course, with no data available on higher levels of damage, further fragility curves could not be plotted.

4. THE LIFETIME PREDICTION FOR MASONRY SUBJECTED TO CREEP-INDUCED DAMAGE

After the collapse of the Civic Tower of Pavia, a XI century building suddenly failed in 1989, approximately 100 large blocks of masonry were recovered for testing from the 7000 m^3 of ruins (Fig. 8). Different types of uniaxial compression tests, including monotonic tests, fatigue tests to simulate the effects of wind, tests applying unloading

Figure 8. Remains of the Civic Tower of Pavia.

reloading cycles were carried out in addition to geotechnical, physical and chemical tests to find the causes of the collapse (Binda et al. 1990*a*). Subsequently, the research focussed on creep and pseudo-creep tests, and to the study of other ancient towers affected by crack patterns indicating a great influence of the self weight (Binda et al., 1991).

4.1. Results of Creep Tests

Six prisms coming from the ruins of the Tower of Pavia were tested in compression in controlled conditions of 20°C and 50% RH, using hydraulic test devices able to keep constant a maximum load of 1000 KN. The dimensions adopted for the prisms (300 mm x 300 mm x 510 mm) were the maximum compatible with the testing machine. The load was applied in subsequent steps, kept constant until either the creep strain reached a constant value or a steady state at relatively low strain-rate was attained. The first stress level was chosen between 40% and 50% of the static peak stress of the prisms.

The static peak stress was estimated by sonic tests (Anzani et al. 2000), according to a relationship between sonic velocity and peak stress resulted by the mechanical testing of prisms previously characterized by sonic tests and similar to that shown in Fig. 13. All the test results are reported in Figure 9.

From the experimental data, the following aspects may be observed:

(i) development of creep strain depending on the stress level, with initial primary creep phase, corresponding to a visco-elastic phase, characterized by reversible strain development at decreasing rate;

(ii) secondary creep - namely a visco-plastic phase characterized by a steady state, with strain developing at constant rate - showing even at 41% of the estimated material peak stress;

(iii) tertiary creep - corresponding to a highly unstable behaviour, characterized by strain developing at increasing rate and definitely ending with the specimen failure - showing at about 70% of the estimated material peak stress;

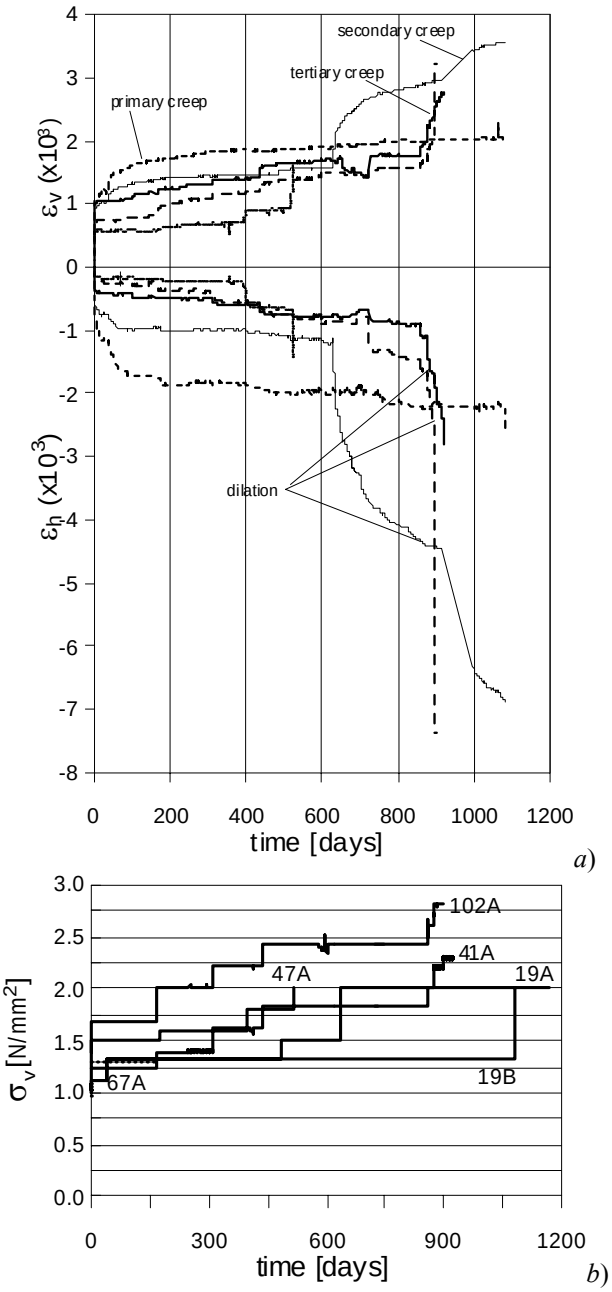

Figure 9. Strain vs. time (a) and stress vs. time (b) diagrams obtained from creep tests

(iv) material dilation under severe compressive stress corresponding to high values of the horizontal strain developing before failure;

(v) slow crack propagation for a long time until failure.

In order to apply the probabilistic model to the interpretation of these experimental data, the vertical and horizontal strain-rate of the secondary creep phase ($\dot{\varepsilon}_v$ and $\dot{\varepsilon}_h$) have been calculated for all specimens at the application of any load step, corresponding to the slope of the linear branch of the strain versus time diagrams. In Figure 10 the crack pattern of a prism at the end of a creep-test is

shown: vertical cracks corresponding to material dilation are visible, mainly passing at the interface between mortar and resistant elements (bricks and stone fragments).

4.2 Results of Pseudo-Creep Tests

In addition to long term tests that require constant thermo-hygrometric conditions and especially designed testing apparatus, a more rapid and therefore more convenient testing procedure was adopted which demonstrated reasonably suitable to study creep behaviour. Four prisms were tested applying the load by subsequent steps corresponding to 0.3 MPa and were kept constant for 28800 sec. Again, the dimensions 200 mm x 200 mm x 350 mm adopted for the prisms were the maximum compatible with the testing machine.

The peak stress obtained by pseudo-creep tests on the masonry of Pavia and on that of the crypt of Monza (XVI cent.) previously tested (Anzani et al., 2005) indicated an interesting direct relationship with the results of sonic tests (Figure 11).

Figure 10. Crack pattern after creep test.

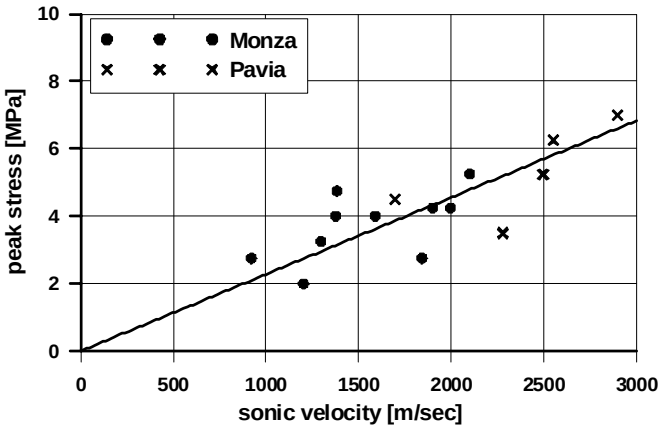

Figure 11. Peak stress vs. sonic velocity.

Stress versus strain and strain versus time diagrams for both vertical and horizontal directions are reported as an example in Figure 12 for one of the prisms tested. As appears from the diagrams, the test procedure allowed obtaining very regular data. As an initial qualitative consideration, it can be observed that the first branch of the stress versus strain diagrams may be considered within the elastic range.

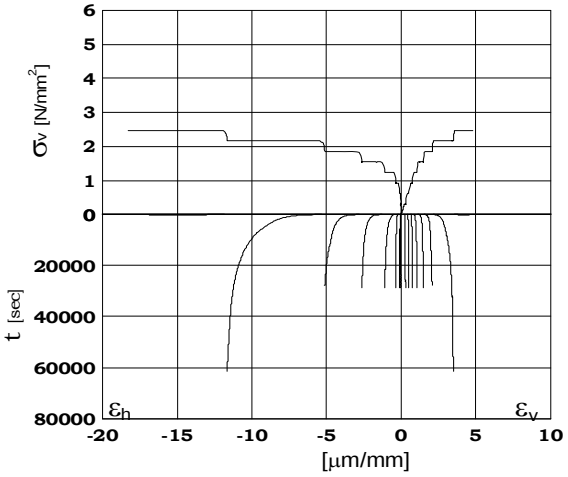

Figure 12. Results of pseudo-creep tests.

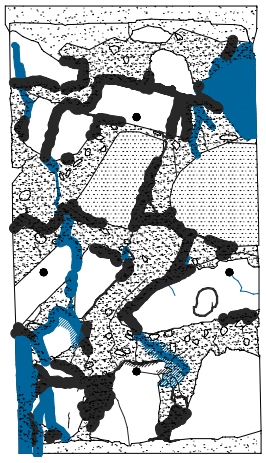

Figure 13. Crack pattern after pseudo-creep test.

The corresponding strain versus time diagrams at every load step only show initial elastic strain (at time = 0) and primary creep strain. Therefore, the slope of the linear branch of the diagrams,

corresponding to the strain-rate, tends to 0. Subsequently, after reaching a stress level of about 1.5 MPa, the stress versus strain diagram departs from a pseudo-linearity and gets a downward concavity, which is particularly evident in the case of horizontal strain. The corresponding strain versus time diagrams start to show also secondary creep strain. Again, this is more pronounced in the case of horizontal strain components: at increasing the stress level, the slope of the linear branch of the diagrams gets progressively higher than 0. Though it is not clearly visible in this case, at the last load step tertiary creep strain takes place.

Figure 13 shows the final crack pattern of a prism subjected to pseudo-creep test: like in Figure 10, vertical and sub-vertical cracks, corresponding to material dilation, are evident mainly passing at the interface between mortar and resistant elements (bricks and stone fragments). Again, the horizontal strain-rate in the secondary creep phase obtained for each specimen at each load step was considered as a significant parameter.

4. 3 Stochastic Modelling of the Creep-Induced Damage

Considering the results of creep and pseudo-creep tests, the strain evolution connected with a given stress history of an ancient masonry can be described through the parameters $\dot{\varepsilon}_v$ and $\dot{\varepsilon}_h$ respectively defined as the vertical and horizontal strain-rate, taken on the linear branches of the strain versus time diagrams shown by the specimen at any stress level σ, remaining constant for a certain time interval.

Taking the experimental measurements of $\dot{\varepsilon}_h$ at discrete stress values σ^*, the p.d.f. $f_{\dot{\mathrm{E}}}(\dot{\varepsilon},\sigma^*)$ depends on the strain-rate $\dot{\varepsilon}$ and on σ^* which is constant at every step, therefore the modeling of the strain-rate behaviour depends only on the random variable $\dot{\varepsilon}$ (Fig. 14). In order to model $\dot{\varepsilon}$, at every stress level σ^* a family of theoretical distributions has to be chosen.

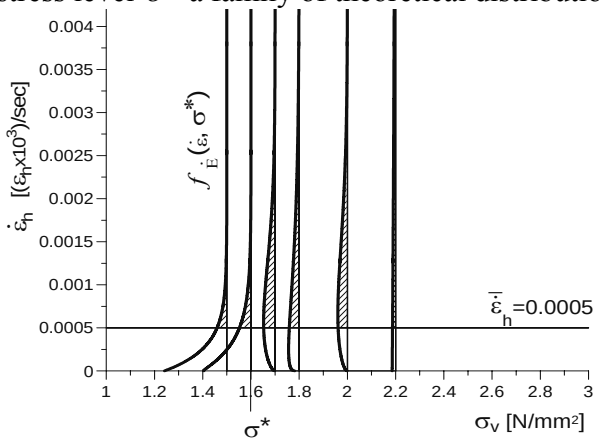

Figure 14. Exceeding probability to cross the threshold $\bar{\dot{\varepsilon}}_h$.

For a given stress level σ^* the probability to record a threshold strain-rate increases if the strain-rate $\dot{\varepsilon}$ increases. Therefore, it seems correct to assume that, at a given stress level σ^* the higher is the strain-rate, the higher is the probability that the secondary creep strain-rate falls within the interval $\left\{\dot{\mathrm{E}} < \dot{\varepsilon} \le \dot{\mathrm{E}} + d\dot{\mathrm{E}}\right\}$. The strain-rate $\dot{\varepsilon}$ at the stress level σ^* has therefore been modelled with an extreme value distribution. Always by experimental evidence, it seems that when σ^* tends to infinite the probability that the secondary creep strain-rate falls within the interval $\left\{\dot{\mathrm{E}} < \dot{\varepsilon} \le \dot{\mathrm{E}} + d\dot{\mathrm{E}}\right\}$ tends to infinite too, therefore a Weibull distribution was considered suitable to model this problem:

$$f_{\dot{\mathrm{E}}}(\dot{\varepsilon}) = \alpha_{\dot{\mathrm{E}}} \rho_{\dot{\mathrm{E}}} (\rho_{\dot{\mathrm{E}}}\ \dot{\varepsilon})^{\alpha_{\dot{\mathrm{E}}}-1} \exp[-(\rho_{\dot{\mathrm{E}}}\ \dot{\varepsilon})^{\alpha_{\dot{\mathrm{E}}}}] \qquad (14)$$

where α and ρ are the parameters of distribution.

This family of distributions presents an immediate occurrence rate function which increases if the value of $\dot{\mathrm{E}}$ increases and tends to ∞ if $\dot{\mathrm{E}} \to \infty$; this fact seems to respect the physical interpretation of the strain-rate behaviour previously commented.

In the modelling of the strain-rate behaviour, the function in Eq. 4 assumes the form:

$$\Im_{\dot{\mathrm{E}}}(\dot{\varepsilon}) = 1 - F_{\dot{\mathrm{E}}}(\dot{\varepsilon}) \qquad \forall \sigma^* \qquad (15)$$

Eqs. 14 and 15 have been applied to model vertical and horizontal strain rate of both creep and

pseudo creep results; the experimental fragility curves obtained by the application of Eq. 15 will be presented in the following paragraphs.

4.3.1 Application of the probabilistic approach to creep tests

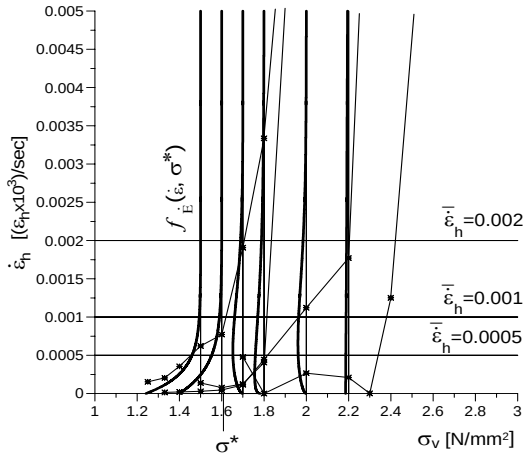

Figure 15. Creep tests, interpolation of the horizontal strain-rate vs. applied stress and the modelling of $f_{\dot{E}}(\dot{\varepsilon}, \sigma^*)$

From the creep tests previously described, the horizontal strain-rate taken on the linear branches of the strain versus time diagrams have been plotted vs. the stress level σ (Figure 15). The diagrams show an initial pseudo-constant branch with low values of the strain-rate, followed by a clearly increasing part that ends with the collapse (Anzani et al. 2003).

For modelling $f_{\dot{E}}(\dot{\varepsilon},\sigma)$, the identification of significant thresholds of critical strain rate is crucial. The choice can be made considering the relationship between the secondary creep strain-rate and the residual life of the material (Taliercio et al. 1996 and Anzani et al. 2000). In order to prevent major damage or even failure, it would be very convenient to indicate a critical value of the strain-rate under which the residual life of the building is conveniently greater than the required service life. In Figure 15, three conventional critical strain-rate values $\bar{\dot{\varepsilon}}_h$ have been identified, corresponding to the initiation and the first development of the secondary creep phase for most of the prisms.

In Figure 16 the experimental and theoretical fragility curves connected with these thresholds are reported. They describe the probability to exceed the critical thresholds as a function of the reached stress level σ_v. In this case the definition of "reliability" is extended and $\bar{R}(\sigma)$ is assumed as the probability that the system does not exceed a given significant strain-rate $\bar{\dot{\varepsilon}}$ with a stress σ. The random variable used to quantify reliability is $\bar{\sigma}$ which is just the stress to exceed the strain-rate $\bar{\dot{\varepsilon}}$. Thus, from this point of view, the reliability function is given by (Garavaglia et al. 2002*b*, Garavaglia et al., 2004*,* Bekker, 1999)

$$\bar{R}(\sigma) = \Pr(\bar{\sigma} > \sigma_v) = 1 - F_{\bar{\sigma}}(\sigma_v), \qquad (16)$$

where $F_{\bar{\sigma}}(\sigma_v)$ is the distribution function for $\bar{\sigma}$ and represents the theoretical modelling of the experimental fragility curves.

Referring to a previous research (Anzani et al., 2003), the same thresholds connected to the initiation of the secondary creep may be indicated also for the vertical strain-rate. In Figure 17 the experimental and theoretical fragility curves related with the thresholds previously adopted for the horizontal strain-rate are shown. In Table 1 a comparison between vertical and horizontal strain-rate is reported.

The optimised estimation of the distributions parameters was obtained by fitting the experimental fragility curves with an error included within the interval 9.5e-03 and 9.9e-02. Though the error is not small as hoped however, since the distribution assumed to model the phenomenon is supported by the physic of the phenomenon itself, is acceptable.

The choice of these three percentage values are related to the limits of an interval of possible previsions (10% – 90%), whereas the value of 63% is related to the born-in method used to test the significance of an experimental test: for a Weibull modeling 63% is the limit describing a reliable prevision because most of the experimental data fall below this limit.

Comparing these results, it can be observed that always the exceedance of the chosen threshold strain-rate is performed at a lower stress level in the case of horizontal strain. This is in good agreement with the dilatant behaviour of ancient masonry when approaching failure, as shown by

Figure 9, where the horizontal strain appears to be higher and developing at a higher rate than the vertical ones. This behaviour is typical of a damaged material presenting a response beyond the elastic limit.

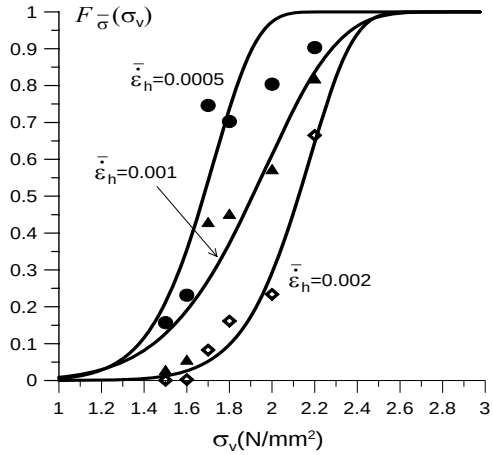

Figure 16 Horizontal strain-rate: experimental (●, ▲, ◊) and theoretical (—) fragility curves from creep-tests.

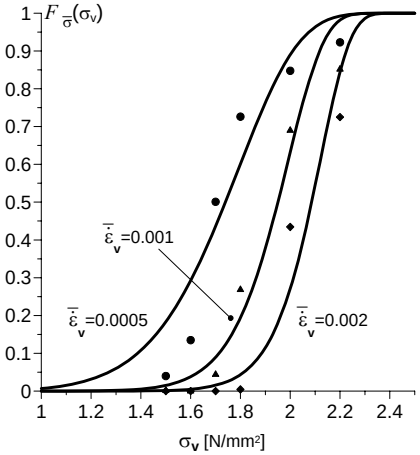

Figure 17. Vertical strain-rate: experimental (●, ▲, ♦) and theoretical (—) fragility curves from creep-tests.

	$\dot{\bar{\varepsilon}}_v = 0.0005$	$\dot{\bar{\varepsilon}}_h = 0.0005$
Exceedance prob. of $\dot{\bar{\varepsilon}}_v$	σ_v (N/mm^2)	σ_v (N/mm^2)
10%	1.40	1.38
63%	1.81	1.75
90%	2.00	1.90

Table 1. Probability to exceed $\dot{\bar{\varepsilon}}_v$ *and* $\dot{\bar{\varepsilon}}_h$ *for different* σ_v

This is also confirmed by Figure 10 where the crack pattern of a prism at the end of creep test is shown: having loaded the specimen vertically in compression, the cracks follow a mainly vertical path, therefore giving an apparent horizontal dilation. However, from a probabilistic point of view, caution must be offered to the tails of the distribution where usually not much data are present and where the prediction becomes critical.

4.3.2. Fragility curve $\dot{\varepsilon}$ **versus** σ *applied to pseudo creep tests*

Also in the case of pseudo-creep tests, threshold strain-rate values connected to the initiation and the evolution of the secondary creep phase were found. The experimental and theoretical fragility curves connected with the thresholds $\dot{\bar{\varepsilon}} = 1.0\text{e}-004$, $\dot{\bar{\varepsilon}} = 1.0\text{e}-004$ and $\dot{\bar{\varepsilon}} = 2.0\text{e}-004$ are reported for both vertical (Fig. 18*a*) and horizontal (Fig. 18*b*) strain-rates.

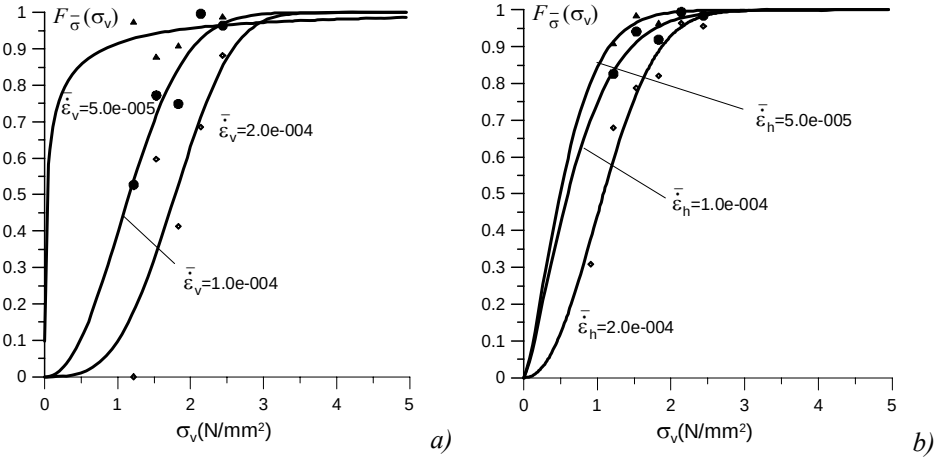

Figure 18. Experimental (▲ - ● - ◊) and theoretical (—) fragility curves obtained from pseudo-creep tests: a) vertical strain; b) horizontal strain.

The optimised estimation of the distributions parameters was obtained by fitting the experimental fragility curves with a maximum error of 0.11 for the threshold $\dot{\bar{\varepsilon}} = 2.0\text{e}-004$ of Figure 18*a*.

It has to be noted that, due to the different load histories, different strain-rate thresholds were found in this case. In fact, pseudo-creep tests were carried out applying the load stepwise starting from zero, therefore the strain-rate evolution started from lower values than in the case of creep tests. In this case the first load step was applied at 40-50% of the peak estimated stress, therefore higher strain-rate values were obtained.

	$\dot{\bar{\varepsilon}}_v = 5.0\text{e}-005$	$\dot{\bar{\varepsilon}}_v = 1.0\text{e}-004$	$\dot{\bar{\varepsilon}}_v = 2.0\text{e}-004$	$\dot{\bar{\varepsilon}}_h = 5.0\text{e}-005$	$\dot{\bar{\varepsilon}}_h = 1.0\text{e}-004$	$\dot{\bar{\varepsilon}}_h = 2.0\text{e}-004$
Exceedance prob.	σ_v *(N/mm²)*	σ_v *(N/mm²)*	σ_v *(N/mm²)*	σ_v *(N/mm²)*	σ_v *(N/mm²)*	σ_v *(N/mm²)*
10%	0.01	0.49	1.03	0.13	0.15	0.46
63%	0.09	1.38	1.99	0.64	0.79	1.28
90%	0.80	2.02	2.58	1.18	1.48	1.87

Table 2. Probability to exceed $\dot{\bar{\varepsilon}}_v$ *and* $\dot{\bar{\varepsilon}}_h$ *for different* σ_v

Comparing these results with those reported in Table 1, despite a certain scatter in the results a tendency similar to that shown by the creep test is confirmed, but here some additional comments have to be made. In the 10% of the cases the exceedance of the chosen threshold strain-rate is performed at a lower stress level in the case of vertical strain. On the contrary, at 63% and 90% of the cases the exceedance of the chosen threshold strain-rate is performed at a lower stress level in the case of horizontal strain, exactly like in the creep test. This indicates that the prisms tested with pseudo-creep still presented a visco-elastic non-dilatant response at low stress level, whereas at higher stress level their behaviour was beyond the elastic limit.

Since the same material has been tested in the two cases, despite the different prism dimensions, the reason has to be found in the different load histories. In fact, in the case of creep tests the first load step corresponded to the 40-50% of the estimated static peak stress, therefore the material was presumably beyond the elastic limit. On the contrary, in the case of pseudo-creep tests the load was applied through small steps therefore, at the initial stage, the material still had to be within the elastic limit, whereas at higher stress level it performed a dilatant response.

If applied to real cases, this type of prediction allows to evaluate, for instance, the results of a monitoring campaign on a massive historic building subjected to persistent load and to judge whether the creep strain indicates a critical condition in term of safety assessment. Significant measurements might be the evolution of geometric parameters like the rate of crack opening, whether a clear crack pattern is visible, or the wall thickness increase rate at the base of the building whether the construction is made of a multiple leaf masonry and characterized by an invisible micro-crack damage. Knowledge of the constant vertical stress value at the monitoring level is also required: flat jack tests can suitably provide direct quantitative data. Of course, the precocious recognition of a critical state will allow to design a strengthening intervention to prevent total or partial failure of the construction.

4.4 Application of the Probabilistic Approach to the Bell Tower of Monza

The proposed probabilistic approach has been applied for the first time to evaluate the results of the monitoring of a massive historic building subjected to persistent vertical loading, mainly originating from self weight. The Bell Tower of Monza, a XVI century structure built in solid brickwork masonry, had suffered major and diffused cracks due to high compression (Fig. 19) (Binda et al., 1998).

After the constitution of a Technical Committee in 1976 the building, together with the Cathedral, was subjected to a systematic control, setting up 31 fixed basis, 7 of which on the Tower corresponding to the major cracks. The measuring basis has a length of about 400 mm, and the measurements were taken, starting in January 1978, every month during the first three years and every three months subsequently. The instrument used was a millesimal deformometer. After the

recorded increase of the crack opening on the Tower and an anomalous geometry recorded on the Cathedral, in 1992 a new Committee was constituted by The DIIAR Politecnico di Milano, who installed a static control system, that included the continuation of the geometric evaluation of the cracks. Each of the previous bases was substituted by a couple of new basis placed above and below the other ones, having a length of 200 mm, the readings being taken at the same periodicity (every three months).

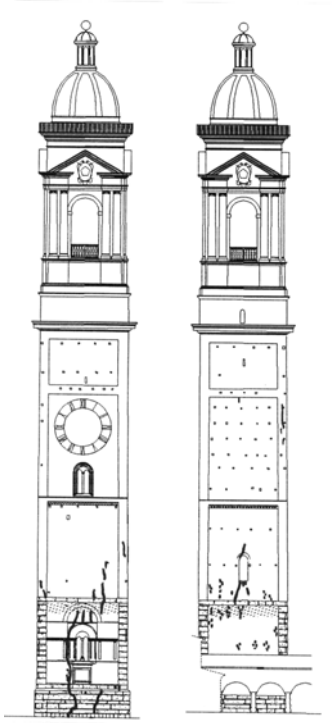

Figure 19. Crack pattern of the Bell Tower of Monza.

Considering the data collected until 1999 (Fig. 20), the influence of thermal variation on the crack opening can clearly be observed. Nevertheless, tracing a regression line through the data, a net increase of the crack opening in time is visible; in the case of the base shown in Figure 20 a rate of crack opening of 6.48 micron/year can be measured until 1986 and a higher rate of 24.94 micron/year can be measured subsequently. This clear worsening of the Tower static conditions could not be attributed to any external reason, so an intrinsic damage may only be assumed. After the static survey, a consolidation intervention on the Tower was decided for, which is still in progress.

In order to compare the rate of crack opening of the Tower with the strain rate measured in the laboratory, the average strain rate was calculated based on the monitoring data. This calculated rate was related with the values of the vertical stress, locally measured by flat jack tests at the same height of the crack monitoring. Flat jack tests gave respectively a vertical stress of 0.98 N/mm^2 at a height of about 12 m and of 1.67 N/mm^2 at a height of about 5 m which were in good agreement with the FE elastic analysis considering the self weight (Binda et al., 1998). The fragility curves shown in Figure 21 were built for the tower cracks for two different thresholds $\bar{\dot{\varepsilon}}_h$ of horizontal strain rate. As expected, in this case the parameter optimisation gives very small errors (7.70e-11 and 3.41e-09 respectively) because only two points were fitted. The recorded strain-rate and stress level, and consequently the chosen threshold strain-rate values, are lower than those obtained by creep and pseudo-creep laboratory tests: in fact, the latter were aimed to take the prisms to failure whereas the tower of Monza is still performing its servicelife. Here the modelling appears hazardous, but on the basis of the results obtained by laboratory tests it is possible to suppose the same distribution (Weibull distribution) for modelling the probability of exceedance of the $\bar{\dot{\varepsilon}}_h$ thresholds chosen. Although two data are not sufficient to investigate the Weibull shape, however the results obtained look like an interesting example of possible application of the procedure at real cases, where more suitable data are available. The decision of strengthening the tower was, of course, taken independently from the present research.

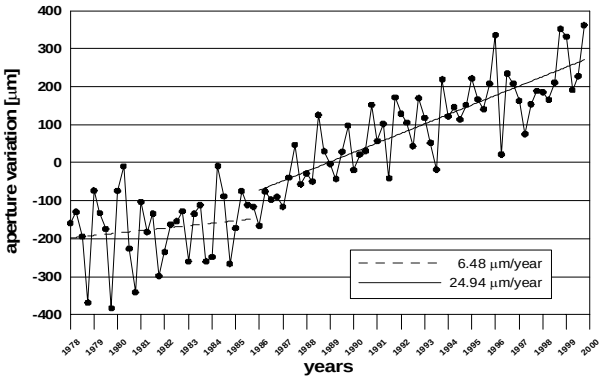

Figure 20. Monitoring of the Bell Tower of Monza: opening variation of a crack vs. time.

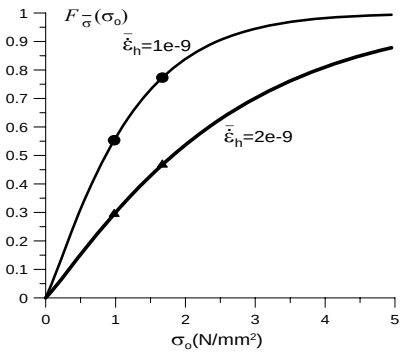

Figure 21. Horizontal strain rate, experimental (• ▲) and theoretical (—) fragility curves.

5. CONCLUSIONS

Considering the great randomness associated to different physical and mechanical decay processes, and the importance of the lifetime prediction for planning maintenance and repair strategies, a probabilistic approach has been successfully applied to study salt decay and creep induced damage of historical masonry.

The deterioration development, considered as a stochastic process, was modelled adopting a Lognormal theoretical distribution in the case of salt decay process and a Weibull distribution in the case of creep induced damage. In both cases, the lifetime prediction was performed thanks to useful applications of the Weibull distribution to model numerically the experimental fragility curves.
In the lifetime prediction of the masonry wallettes subjected to crystallization test, the results obtained show that the approach proposed is able to predict, in probabilistic terms, the magnitude of the expected damage over time and the occurrence time for a given damage level. Therefore, through the model the effectiveness of treatment on different building materials can suitably be evaluated. The model prediction seems to be confirmed by the real behaviour of the wallettes, also in the case where no surface damage was visible.

In the lifetime prediction of masonry subjected to long term heavy loads, the chosen model seems to appropriately interpret the experimental results also capturing the evolution of visco-elastic to visco-plastic behaviour. An attempt of applying the procedure to the results of long term monitoring of displacements, particularly of crack opening, was carried out. Though the experimental data were too few to achieve a statistically reliable result, however an interesting indication for possible interpretation of long-term monitoring data has been highlighted.

Acknowledgement

C. Tedeschi, B. Lubelli, R. Tassi and S. Sironi are gratefully acknowledged for the experimental activity; many thanks to M. Antico for the technical support and to C. Arcadi for the precious and constant help.

REFERENCES

Anzani, A., Binda, L., Garavaglia, E. (2003). The vulnerability of ancient buildings under permanent loading: a probabilistic approach, *Proc. of 2nd Int. Symp. ILCDES 2003, Integrated Life-Cycle Design of Materials and Structures*, Kuopio, Finland, RIL/VTT Ed., Helsinki, Finland, UE., **I**, 263 – 268.

Anzani, A., Binda, L., Mirabella Roberti G. (2000). The effect of heavy persistent actions into the behaviour of ancient masonry, Materials and Structures, **33**, 251 – 261

Anzani A., Garavaglia E., Binda L., (2005). A probabilistic approach for the interpretation of long term damage of historic masonry, *Proc. of 10th Canadian Masonry Symposium*, Banff, Alberta, Canada, June 8 – 12, 2005, Ed. S. Lissen, C. Benz, M. Hagel, C. Yuen, N. Shrive, Printed by Dept. of Civil Eng. The University of Calgary, Canada, **I,** 664 – 673.

Augusti, G., Baratta, S., Casciati, F. (1984). *Probabilistic Methods in Structural Engineering*, Chapman and Hall, London, UK.

Baronio, G., Binda, L., Cantoni, F., Rocca, P., (1993). Durability of stone and Brick-work protectives and consolidants: experimental research on full-scale models, *6th Int. Conf. on Durability of Building Materials and Components*, Omiya, Japan, Vol. **2**, pp. 824-833.

Bekker, P.C.F., (1999). Durability testing of masonry: statistical models and methods, *Masonry International,* **13**(1), 32-38.

Berra, M., Fatticcioni, A., Binda, L., Squarcina, T., (1993). Laboratory and in-situ measurements procedure of the decay of masonry surfaces, *6th Int. Conf. on Durability of Building Materials and Components*, Omiya, Japan, Vol. **2**, pp.834-843.

Binda L., Anzani A., Gioda G., (1991). An analysis of the time-dependent behaviour of masonry walls, *9th Int. Brick/Block Masonry Conf.*, Berlin, vol. 2, 1058-1067.

Binda, L., Anzani, A., Mirabella Roberti, G. (1997). The failure of ancient towers: problems for their safety assessment, *Conf. on Composite Construct. - Conventional and Innovative*, IABSE, Insbruck, **I**, 699 – 704.

Binda, L., Baronio G., (1985). Alteration of the Mechanical Properties of Masonry Prisms due to Aging, *7th IBMaC*, Melbourne, Australia, **1**, 605-616.

Binda L., Baronio G., Lubelli B., Rocca P., (1999*a*). Effectiveness of surface treatments of stone and brick masonry: proposal and calibration of on site control techniques, *Proc. of 8DCMC*, *8th International Conference on*

Durability of Building Materials and Components, Vancouver, Canada, **1**, 538-549.

Binda, L., Baronio, G., Lubelli, B., Rocca, P., (1999*b*). "Effectiveness of surface treatments of stone and brick masonry: proposal and calibration of on site control techniques." *Proc. of 8DCMC, 8th International Conference on Durability of Building Materials and Components*, Vancouver, Canada, M. A. Lacasse, D. J. Vanier Editors, NRC-CNRC, Ottawa, Canada, **1**, 538-549.

Binda, L., Baronio, G., Squarcina, T., (1992). Evaluation of the durability of bricks and stones and of preservation treatments, *7th Int. Congr. of Deterioration and Conservation of Stone,* Lisbon, Portugal, Vol. **2**, pp. 753-761.

Binda, L., Charola, A.E., Baronio, G., (1985). Deterioration of porous materials due to salt crystallisation under different thermohygrometric conditions, *5th Int. Conf. on Deterioration and Conservation of Stone*, Lausanne, Suisse, **I**, 279-288.

Binda, L., Gatti, G., Mangano G., Poggi, C. & Sacchi Landriani, G. (1990*a*). La Torre Civica di Pavia: indagini sui materiali e sulla struttura, L'Edilizia e L'Industrializzazione, **11**, 713 – 735.

Binda, L., Molina, C., (1990*b*). Building Materials Durability Semi-Markov Approach. *J. of Materials in Civil Engineering*, ASCE, USA., **2**(4), 223–239.

Binda, L., Tiraboschi, C., Tongini Folli, R., (1998). On site and laboratory investigation on materials and structure of a Bell-Tower in Monza*, 2nd Int. Conf. RILEM on Rehabilitation of Structures*, Highett, Melbourne, Australia, **I**, 542-556.

Cardani G., Tedeschi, C., Binda L., Baronio G., (2002). Crystallisation Test on Treated Brick/Stone Masonry Specimens for Damage Evaluation", *Int. Conf. 9th Durability of Building Materials*, 17-20 March, 2002, Brisbane, Queensland, Australia, Paper n. 039, CD-ROM.

Cox, D.R., (1962). *Renewal Theory*, Methuen LTD, London, UK, EU.

Cranmer D.C. & Richerson D.W., (1998). *Mechanical Testing Methodology for Ceramic Design and Reliability*, Marcel Dekker, New York, NJ, USA.

Evans, D.H., (1992). *Probability and its Applications for Engineers*. Marcel Dekker Inc., New York, NJ, USA.

Garavaglia, E., Anzani, A., Binda, L. (2004*a*). A probabilistic model for the assessment of historic buildings under permanent loading" *Proc. of SAHC IV Int. Seminar On Structural Analysis of Historic Constructions – Possibilities of numerical and experimental techniques,* Padua, Italy. EU, **I**, 589-596.

Garavaglia E., Cardani G., Binda L. (2002*a*). A probabilistic model to predict the durability of surface treatments", *Int.l J. of Restoration of Buildings and Monuments/Internationale Zeitschrift für Bauinstandsetzen und Baudenkmalpflege*, Ed. Aedificatio Verlag, Freiburg, **8**(2/3), 223-254.

Garavaglia, E., Gianni, A., Molina, C. (2004*b*). Reliability of porous materials: two stochastic approaches" *J of Materials in Civil Engineering*, ASCE, **16**(5).419-426.

Garavaglia, E., Lubelli, B., Binda, L., (2002*b*). "Two different stochastic approaches modelling the deterioration process of masonry wall over time." Materials and Structures, RILEM Pubblications s.a.r.l., EU, **35**(248), 246-256.

Howard, R.A., (1971). *Dynamic probabilistic system*. John Wiley and Sons, New York, NJ, USA.

Maybeck P.S., (1979) *Stochastic Models, Estimation, and Control Vol. 1*, Series of Mathematic in Science and Engineering, Academic Press, New York, NJ, USA.

RILEM MS. A.1, (1998). Determination of the resistence of wallettes against sulphate and chloride, Materials and Structures, **31**, 2-19.

Singhal A., Kerimidjian A.S. (1996). "Method for Probabilistic Evaluation of Seismic Structural Damage." *J. of Structural Engineering*, ASCE, USA., **122**(12), 1459-1467.

Taliercio, A.L.F. & Gobbi, E. (1996). Experimental investigation on the triaxial fatigue behaviour of plain concrete, *Magazine of Concrete Research*, **48**(176), pp. 157 – 172.

Van Hees, R.P.J., Koek, J.A.G., De Clercq, H., De Witte, E., Binda, L., (1996). Evaluation of the performance of surface treatments for the conservation of brick masonry, *8th Int. Congr. on Deterioration and Conservation of Stone*, Berlin, Germany, Vol. **3,** pp. 1695-1715.